Pure and binary adsorption of carbon dioxide and nitrogen on AQSOA FAM Z02

Pure and binary adsorption of carbon dioxide and nitrogen on AQSOA FAM Z02

Charithea Charalambous[†], *Giulio Santori*[*,†], *Enrique Vilarrasa-Garcia*[‡], *Moises Bastos-Neto*[‡], *Célio L. Cavalcante Jr.*[‡], *Stefano Brandani*[†]

[†]The University of Edinburgh, School of Engineering, Institute for Materials and Processes, Sanderson Building, The King's Buildings, Mayfield Road, EH9 3FB, Edinburgh, Scotland, UK.
[‡]Universidade Federal do Ceará, Departamento de Engenharia Quimica, Grupo de Pesquisa em Separações por Adsorção, Campus do Pici, Bl. 709, 60455-760 - Fortaleza, CE, Brasil.

ABSTRACT. Adsorption equilibria of CO_2, N_2 and CO_2/N_2 binary system on AQSOA FAM Z02 grains were measured at a temperature range of 295 K to 348 K and over a wide range of pressure from 0.2 bar to 20 bar using a gravimetric method. CO_2 and N_2 single component experimental equilibrium measurements were regressed using the Toth equation. CO_2 adsorption on AQSOA FAM Z02 reported higher loadings compared to N_2 adsorption at all measured temperatures with an adsorption capacity of 6.1 mmol g^{-1}. Adsorption of CO_2/N_2 binary mixture at different gas phase compositions (0.15/0.85, 0.50/0.50 and 0.80/0.20 mole fraction) was studied. The experimental data were compared with the prediction of ideal adsorbed solution theory (IAST), which included also the non-idealities in the bulk-gas phase. The IAST model has shown an agreement with the experimental data with < 4 % average relative error in the absolute adsorbed amount.

1. INTRODUCTION

Capture of carbon dioxide by adsorptive processes is based on preferential adsorption of carbon dioxide on porous adsorbents from dilute gas streams. Several review have compared the features of different solid adsorbents for carbon capture such as activated carbons, zeolites, metal organic frameworks, silica and polymers of intrinsic porosity [1–3]. Optimal performance of any adsorption separation process is enabled by materials with large CO2 working capacity and selectivity over the additional components in the mixture and ideally long cycle lifetime. [4] In industrial processes, zeolite 13X is frequently used as an adsorbent due to its high adsorption capacity[5,6] and high CO_2 selectivity over other gases.[7–9] Although, when H_2O is present in the mixture, in applications such as CO_2 capture from flue gases and CO_2 removal in closed-circuit breathing systems, it adsorbs near its pure component isotherm [10] making zeolite 13X an unfavorable sorbent for carbon dioxide removal applications. Alternatively, the initial stream has to undergo preliminary drying, which removes nearly 99.9% of water from the mixture before further treatment. Consequently, the drying step adds a cost to the gas separation process and it is most likely not feasible on large scale applications.[11]

Ideally, an adsorbent with a hydrophobic nature or with a relatively low uptake from low to moderate levels of humidity, which follows an unfavorable adsorption isotherm or the type III and V isotherms according to the IUPAC classification of adsorption isotherms,[12] can be superior for carbon dioxide separation and purification processes.

The Functional Adsorbent Material Zeolite, (FAM Z-series), commercialized by Mitsubishi Plastics Inc., show most advantageous adsorption isotherms when contacted with water. [13] AQSOA®-FAM-Z02, based on the SAPO-34 zeotype with CHA-structure, hereafter referred in this paper as AQSOA-Z02, shows very suitable adsorption characteristics — a type V adsorption

isotherm as investigated by Goldsworthy[14] and by Wei Benjamin Teo et al. [15] — to recover CO_2 from a gas mixture containing H_2O. Due to the stepwise uptake of water, partial pressure of water has to exceed a threshold value before water can be adsorbed. This is a feature of AQSOA-Z02 that makes it more favorable than other benchmarking materials such as Zeolite 13X which instead shows type I isotherm for water with very steep trend at low pressure.

A low humidity content feed can be found in applications such as the CO_2 removal from the atmospheric air [16] and from the closed cabin atmospheres [17] to sustain the quality of the breathing air. There, CO_2 exists in the feed stream in parts per million (ppm) while N_2 and O_2 are the main components of the fluid. In order to study the separation of CO_2 for these applications, at least the adsorption of CO_2, N_2 and H_2O on the selected adsorbent is required. Hence, a study on the adsorption equilibrium of carbon dioxide, nitrogen, and carbon dioxide–nitrogen mixtures on AQSOA-Z02 was carried out with a gravimetric apparatus from vacuum to high pressures. The Toth isotherm model and the ideal adsorbed solution theory (IAST) in conjunction with Toth model were applied to describe single component and mixture equilibria. Consequently, this step adds a cost to the gas separation process.

2. EXPERIMENTAL METHODS

MATERIAL. Adsorption of carbon dioxide, nitrogen, and carbon dioxide – nitrogen binary system of: *(i)* 15 mol% CO_2 and 85 mol% N_2, *(ii)* 50 mol% CO_2 and 50 mol% N_2, and *(iii)* 80 mol% CO_2 and 20 mol% N_2 on AQSOA-FAM-Z02 are reported. The adsorbent is a CHA-type (silico)aluminophosphate in the form of loose grains sizes ranging from 0.25–0.45 mm.[18,19] The

physical properties of the adsorbent material are given in Table 1. CO_2 (99.6%) and N_2 (99.995%) were obtained from White Martins-Praxair (Brazil).

Table 1. Physical and surface properties of AQSOA FAM Z02.

Material Property	Value	Reference
Crystal size [μm]	5–10	in [20]
Specific surface area [m^2 g^{-1}]	650–770	in [20]
Mean pore diameter [nm]	0.38	in [13]
Pellet particle density (ρ_{pellet}) [g cm^{-3}]	1.081 [a]	—
Skeleton density (ρ_{sk}) [g cm^{-3}]	2.256 [a]	—
Micropore volume (V_{micro}) [cm^3 g^{-1}]	0.279 [a]	—
Macropore volume (V_{macro}) [cm^3 g^{-1}]	0.203 [a]	—

[a]Data measured in the Adsorption Laboratory of the University of Edinburgh. Micropore volume measurement confirmed data disclosed in ref (21). Macropore volume is calculated from experimental quantities as: $V_{macro} = (1/\rho_{pellet}) - V_{micro} - (1/\rho_{sk})$

MATERIAL SKELETON DENSITY AND POROSITY. A Quantachrome UltraPyc 1200e He pycnometer was used to determine the skeleton density or non-accessible specific volume of the sample. [22] A NIST certified stainless steel sphere of volume 7.07 cm^3 was used to calibrate the volume of the cell. The cell was calibrated with and without the sphere prior to the collection of data.

Once the sample was regenerated at 473 K under vacuum for 2 hr, in an outgassing station of an Autosorb iQ, 4.37 g of the sample was loaded into the cell. A purge step was carried out for 3 mins to evacuate the pores of the sample and the cell. After the purge step, 10 volume measurements were carried out and the results of the last 5 runs were collected and averaged to calculate the skeleton density, which is given in Table 1.

An Autosorb Poremaster mercury porosimeter was used to measure the volume of the macropore of the sample. 1.03 g of regenerated sample was loaded into a porosimeter cell and the procedure, as described by Brandani et al. [22], was followed for the investigation of the pellet density and macro- pore volume. From these results, the micropore volume was calculated. The outcomes are summarized in Table 1.

GRAVIMETRIC APPARATUS. The adsorption experiments were performed using a Rubotherm (Bochum, Germany) magnetic suspension microbalance equipped with a gas mixture dosing unit.

The sample was exposed to the measuring atmosphere while the balance was located outside this atmosphere under ambient conditions, which was achieved using a magnetic suspension coupling, as described by Weireld et al.[23]. Pure component experiments were performed using the two-position mode of the permanent magnet, the so-called ”*Zero Point Position*” and ”*Measuring Point Position*”. The mass at zero point position was calibrated and tared for more accurate weight measurements and the data at both positions were used to correct the buoyancy effect. A comprehensive description of the experimental apparatus and the measurement procedure is given by Dreisbach et al.[24].

Around 0.5 g of adsorbent was outgassed at 473 K until no mass variation in the system was observed and then cooled down to experimental temperature while the gas pressure was increased stepwise until a 20 bar maximal pressure was reached. Mass variation at equilibrium was recorded for each pressure step. Pure component measurements were performed using the gravimetric setup described by Bezerra et al.[25].

The three-position mode automatic magnetic suspension microbalance, consisting of the "*Zero Point Position*", "*Measuring Point 1*" and "*Measuring Point 2*" positions, with an automatic gas mixture dosing system [26] was used for binary mixture adsorption equilibria measurements and density determination, where a titanium sinker was added to the sample container as demonstrated in previous reports[27, 28]. By lifting up the sample holder (measuring point 1 position), the sorption measurement was collected and by raising and weighing the Ti sinker (measuring point 2 position), the density of the fluid phase was determined.

A procedure similar to that used for the regeneration of the adsorbent in the two-position magnetic suspension balance was also implemented on the three-position balance prior to the recorded data. The peripherals and magnetic suspension coupling were operated automatically using MessPro software (Rubotherm) for the collection of adsorbed mass and density at each pressure step at isothermal conditions.

DATA ANALYSIS. Since adsorption data were obtained gravimetrically, the balance reading $m_{Bal}(p, T)$ has to be corrected due to the buoyancy effects acting on the adsorbent and components of the balance holding the sample by

$$m_{Bal,Corr}(p,T) = \Delta m_{spec}(p,T) + (V_s + V_{sc})\rho(p,T) \quad (1)$$

where $m_{Bal,Corr}$ [g] denotes the mass of adsorbate after buoyancy correction, V_s [cm^3] represents the specific volume of adsorbent sample displacing the atmosphere, V_{sc} [cm^3] is the volume of the balance suspended components, ρ [g cm^{-3}] denotes the density of the atmosphere surrounding the sample, p [bar] is the pressure, and T [K] is the temperature.

Δm_{spec} [g] indicates the specific mass change of the sample due to adsorption. This was governed by

$$\Delta m_{spec}(p,T) = m_{Bal,Corr}(p,T) - m_{sc}(p,T) - m_s(p,T) \quad (2)$$

where m_{sc} [g] is the mass of the sample container in vacuum obtained from blank measurement without sample and m_s [g] denotes the mass of reactivated sample calculated in the loading and reactivation of sample step with an inert gas. Information about the blank measurement and the loading and reactivation of sample steps can be found in Weireld et al.[23]. V_{sc} in eq (1) does not depend on pressure and was measured in a calibration experiment without sample.[24]

By considering V_s as equal to the skeleton volume (V_{sk}), the surface excess adsorbed amount was evaluated. Although, to model adsorption processes, absolute adsorption has to be determined as stated by Brandani et al. [22] and Myers and Monson [29]. The difference between the absolute and the excess adsorption was governed by

$$q^{abs} = q^{exc} + \frac{\rho_g V_{ads}}{m_s M_w} \quad (3)$$

Where q^{abs} [mol kg^{-1}] represents the absolute adsorbed amount, q^{exc} [mol kg^{-1}] denotes the excess adsorbed amount, ρ_g [g cm^{-3}] is the density of the gas phase, V_{ads} is the pore volume participating to the adsorption [cm^3], equivalent to the micropore volume in the present work, and M_w [kg mol^{-1}] is the molecular mass of the gas.

By considering the volume of the adsorbed layer, V_s in eq (1) becomes the volume of the solid including micropores, which cannot be measured directly in the same experimental setup. This value can be obtained experimentally by measuring the volume of the skeleton and the volume of the micropores (V_{micro}) independently. V_{sk} was measured in the same gravimetric system by carrying out experiments with an inert gas. In this work, helium was used for V_{sk} determination. Another alternative to examine the non-accessible volume of the sample was implemented using a helium pycnometer (HeP) as has been previously described. The volume of the adsorbed layer or else V micro was calculated from

$$\mathrm{V_{micro}} = \mathrm{V_s} - \mathrm{V_{sk}} = (\mathrm{V_{pellet}} - \mathrm{V_{macro}})_{HgP} - (\mathrm{V_{sk}})_{HeP} \quad (4)$$

where the volume of the pellet V_{pellet} [cm^3] and the volume of the macropores V_{macro} [cm^3] were obtained by means of mercury intrusion porosimetry (HgP) .

ERROR ANALYSIS. The parameters that theoretically affect the sorption measurements followed

$$q^{abs} = f(m_{Bal}, m_{sc+s}, m_s, \dot{v}_i, P, T, V_{micro}) \quad (5)$$

where $\dot{v}_i$ [ml min^{-1}] denotes the measured volumetric flow rate of species *i* in the fluid gas.

Table 2. Uncertainties in measurements.

Property	Parameter value	Reference
Standard deviation of mass reading [mg]	± 0.02	[30]
Standard deviation of mass of the solid [g]	± 0.001	[31]
Standard uncertainty in temperature [K] [a]	± 2	–
Accuracy of pressure measurements [%] [a]	± 1	–
Accuracy of gas dosing [% FS]	± 0.04 [b]	[30]
Uncertainty in density measurement	± (0.02 % + 0.01 kg m^{-3})	[30]
Uncertainty in micropore volume [cm^3 g^{-1}]	± 0.001 [c]	[32]

[a] The temperature is measured beneath the sample in the measuring cell using a platinum resistance probe (Pt-100). Pressure measurements are also carried out in the measuring cell. The full pressure range of the balance used for single-component measurements is 200 bar. The balance used for multicomponent adsorption is equipped with two sensors: one up to 10 bar and a second up to 40 bar.

[b] Full scale error is considered as 100 ml min^{-1}.

[c] Considering ± 0.2% volume accuracy in gas pycnometer and ± 9 10^{-5} cm^3 volume resolution in mercury porosimeter as obtained from the supplier Quantachrome Instruments.

To determine the effect of each parameter on uncertainty in the absolute adsorbed amount, the partial differentials of the independent errors were calculated by

$$\delta V_{sc+s} = f(m_{Bal}, m_{sc+s}, \rho) = \left[\left(\left(\frac{\partial V_{sc+s}}{\partial m_{Bal}}\right)\delta m_{Bal}\right)^2 + \left(\left(\frac{\partial V_{sc+s}}{\partial m_{sc+s}}\right)\delta m_{sc+s}\right)^2 + \left(\left(\frac{\partial V_{sc+s}}{\partial \rho}\right)\delta \rho\right)^2\right]^{0.5} \quad (6)$$

$$\delta\rho = f(P,T,y) = \left[\left(\left(\frac{\partial\rho}{\partial P}\right)\delta P\right)^2 + \left(\left(\frac{\partial\rho}{\partial T}\right)\delta T\right)^2 + \sum_{i=1}^{2}\left(\left(\frac{\partial\rho}{\partial y}\right)\delta y\right)^2\right]^{0.5} \quad (7)$$

$$\delta\Delta m_{spec} = f(m_{Bal}, m_s) = \left[\left(\left(\frac{\partial\Delta m_{spec}}{\partial m_{Bal}}\right)\delta m_{Bal}\right)^2 + \left(\left(\frac{\partial\Delta m_{spec}}{\partial m_s}\right)\delta m_s\right)^2\right]^{0.5} \quad (8)$$

Here, V_{sc+s} [cm^3] is the volume of the sample container and the solid and y_i denotes the molar fraction of species i in the fluid gas. Eq (7) is considered for multicomponent adsorption measurements. For pure component mixtures, the term δy_i is excluded.

Therefore, the dependent errors in excess and absolute adsorbed amount were calculated as follows

$$\delta q^{exc} = f\left(\Delta m_{spec}, \rho, V_{sc+s}, m_s\right) = \left(\frac{\partial q^{exc}}{\partial \Delta m_{spec}}\right)\delta\Delta m_{spec} + \left(\frac{\partial q^{exc}}{\partial \rho}\right)\delta\rho + \left(\frac{\partial q^{exc}}{\partial V_{sc+s}}\right)\delta V_{sc+s} + \left(\frac{\partial q^{exc}}{\partial m_s}\right)\delta m_s \quad (9)$$

$$\delta q^{abs} = f(q^{exc}, \rho, V_{micro}) = \left(\frac{\partial q^{abs}}{\partial q^{exc}}\right)\delta q^{exc} + \left(\frac{\partial q^{abs}}{\partial \rho}\right)\delta\rho + \left(\frac{\partial q^{abs}}{\partial V_{micro}}\right)\delta V_{micro} \quad (10)$$

Table 2 represents the uncertainties in the characteristic data. The accuracy of the gas dosing system and the uncertainty in density measurements were considered only for the multicomponent adsorption equilibrium measurements. The uncertainty for the density measurement over the whole temperature and pressure range of the apparatus was given by Rubotherm GmbH [30]. This followed

$$\frac{\Delta\rho}{\rho} \leq \pm[0.02\% + 0.01\ kg\ m^{-3}] \quad (11)$$

At very low densities, the relative part of eq. (11) (0.02%) is negligible compared to the absolute part (0.01 kg m^{-3}). The absolute part would in fact result in a very high relative error, especially for densities below 10 kg m^{-3} as discussed in ref (33).

3. ANALYTICAL ISOTHERM MODEL AND DATA FIT

PURE COMPONENT DATA FIT. The reported pure CO_2 and N_2 adsorption equilibrium data on AQSOA-FAM-Z02 were regressed using the semi-empirical Toth isotherm model. The Toth isotherm was selected since the Toth equation is valid at the low and high end of the pressure range. This is because the equation agrees with the Henry law at low pressure and has a finite limit when the pressure is sufficiently high.[34] The Toth equation was governed by

$$q = q_s \frac{b(T)f}{[1+(b(T)f)^t]^{1/t}} \quad (12)$$

where q [mol kg^{-1}] represents the amount adsorbed, q_s [mol kg^{-1}] denotes the monolayer adsorption capacity, $b(T)$ [bar^{-1}] and t are the temperature dependent parameters, and f [bar] is the fugacity of the adsorbate in the gas phase. The parameters b and t are specific for adsorbate-adsorbent pairs, where the parameter t characterizes the system's structural heterogeneity in adsorbent micropores. For t = 1 the isotherm reduces to the fundamental Langmuir adsorption isotherm equation and further away from unity the system is supposed to be more heterogeneous.[35] The knowledge of the adsorption equilibrium and isosteric heat of adsorption is essential for proper design and operation of any gas-phase adsorption process. The differential adsorption enthalpy (or isosteric heat of adsorption) $\Delta\bar{h}$ [kJ mol^{-1}] for pure fluids can be determined by solving the Clausius-Clapeyron relation:

$$-\frac{\Delta\bar{h}}{R_g T^2} = \left(\frac{\partial lnf}{\partial T}\right)_q \quad (13)$$

A temperature-dependent expression for the fugacity f is obtained by inversion of the Toth isotherm and by expressing the heterogeneity constant t and the adsorption affinity b with temperature-dependent correlations. The adsorption affinity b follows the form:

$$b = b_0 \, exp\left(\frac{E}{R_g T}\right) \quad (14)$$

where b_0 [bar^{-1}] is the pre-exponential factor, E [kJ mol^{-1}] is the monolayer heat of adsorption, R_g [kJ mol^{-1} K^{-1}] is the universal gas constant. By letting general the expression for the heterogeneity coefficient t, the following is the differential enthalpy from Toth isotherm:

$$-\frac{\Delta\bar{h}}{R_g T^2} = \frac{E}{R_g T^2} + \left(\frac{dt}{dT}\right)\left[\frac{1}{t}\left(\frac{ln\left(q/q_s\right)}{1-\left(q/q_s\right)^t}\right) + \frac{1}{t^2} ln\left(\left(q_s/q\right)^t - 1\right)\right] \quad (15)$$

When the heterogeneity coefficient t is temperature independent, the differential enthalpy reduces to the monolayer heat of adsorption. The parameters obtained from the regression of single component data, i.e. q_s, b_0, E, and t allow precise prediction of the mixture adsorption equilibria. Even small errors in the single component adsorption isotherm fitting can result in large errors in the description of multicomponent adsorption, especially in the low-coverage pressure range.

MULTICOMPONENT DATA FIT. Multicomponent adsorption equilibrium data was predicted using the ideal adsorbed solution theory (IAST).[29] The bulk-gas phase was assumed to be non-ideal and therefore, the subsequent system of equations for N_C components was

$$P_{bulk}\, y_i\, \varphi_i = f_i^0\, x_i \quad (16)$$

$$\psi_i = \int_0^{f_i^0} \frac{n_i^0(f_i)}{f_i} df_i \quad (17)$$

$$1 - \sum_{i=1}^{N_c} x_i = 0 \quad (18)$$

$$\frac{1}{n_t} = \sum_{i=1}^{N_c} \frac{m_i}{n_i^0\left(f_i^0\right) M_{w_i}} = 0 \quad (19)$$

P_{bulk} [bar] denotes the bulk pressure, y_i and x_i are the concentrations of species i in the bulk-gas phase and adsorbed phase respectively, φ_i is the fugacity coefficient of the ith component, f_i^0 [bar] and n_i^0 [mol kg^{-1}] are the pure component fugacity in the adsorbed phase and the pure amount adsorbed of species i at the same temperature and reduced grand potential ψ_i [mol kg^{-1}] of the

mixture, n_t [mol kg^{-1}] denotes the total amount adsorbed and m_i is the mass fraction of species *i* in the adsorbed phase.

IAST states that each component in the adsorbed phase has the same reduced grand potential at equilibrium[36] and therefore,

$$\psi = \psi_1 = \cdots = \psi_{N_C} \tag{20}$$

For the case of a binary mixture, the Toth model has an analytical expression for reduced grand potential, but the pure component hypothetical fugacity had to be determined from a numerical method. The Toth expression of reduced grand potential was given by

$$\psi_i = f_i^0 \, q_s \, b_i \; {}_2F_1\left(\frac{1}{t_i}; \frac{1}{t_i}; \left(1+\frac{1}{t_i}\right); -\left(f_i^0 \, b_i\right)^{t_i}\right) \tag{21}$$

where ${}_2F_1$ is the Gauss hyper-geometric function ${}_2F_1$.[37]

4. RESULTS AND DISCUSSION

PURE COMPONENT ADSORPTION EQUILIBRIA. Pure CO_2 and N_2 component data on AQSOA-FAM-Z02 was measured at (298.15, 323.15, and 348.15) K and pressure range from 0.2 to 20 bar. All measured and treated CO_2 and N_2 equilibrium data are presented in Tables 3 and 4. The best fitting parameters of single component data were obtained by performing a weighted fit to the definition of sum of squares due to error (SSE). To apply this method, weights were added to the definition of the sum of residuals divided by the sum of weights to normalize the objecting function as follows

$$f(q_s, b, t) = \frac{\sum_{i=1}^{N_{data}} \left[w_i (q_{exp} - q_{theor}(q_s, b, t))\right]^2}{\sum_{i-1}^{m} w_i} \tag{22}$$

where $w_i = (i+1)^{-1}$ is the ith weighting factor, q_{exp} [g g^{-1}] is the ith experimental absolute adsorbed amount, q_{theor} [g g^{-1}] is the ith model-predicted adsorbed amount obtained from the Toth equation, and N_{data} denotes the number of pressure steps (observations) at each isotherm.

The objective function $f_s(q_s, b, t)$ was then minimized using the non-linear Conjugate Gradient model and b_0 and E parameters were calculated from eq. (14).

The regressed parameters of the proposed model for describing pure adsorption isotherms and their estimated uncertainties are presented in Table 5. Experimentally collected adsorption isotherms of carbon dioxide and nitrogen on AQSOA-FAM-Z02 were plotted against the Toth equation and are illustrated in Figure 1.

Table 3. Experimental CO_2 adsorption equilibrium data.

298 K		323 K		348 K	
f [bar]	q^{abs} [mol kg^{-1}]	f [bar]	q^{abs} [mol kg^{-1}]	f [bar]	q^{abs} [mol kg^{-1}]
0.005	0.058	0.200	0.482	0.200	0.220
0.010	0.102	0.579	1.124	0.499	0.542
0.021	0.182	0.996	1.652	0.997	0.992
0.028	0.239	1.492	2.058	1.493	1.366
0.039	0.309	1.985	2.371	1.988	1.600
0.048	0.368	2.966	2.811	2.983	1.994
0.058	0.429	4.915	3.332	4.946	2.511
0.068	0.489	6.842	3.655	6.866	2.856
0.079	0.547	10.546	4.047	10.647	3.306
0.087	0.592	14.152	4.281	14.346	3.563
0.099	0.650	18.501	4.516	18.843	3.855
0.199	1.062				
0.299	1.382				
0.398	1.639				
0.500	1.865				
0.600	2.056				
0.699	2.219				
0.799	2.364				
0.900	2.499				
0.993	2.609				
1.489	3.081				
1.980	3.367				
2.965	3.752				
4.896	4.170				
6.758	4.421				
10.443	4.728				
13.905	4.916				
18.046	5.068				

Table 4. Experimental N_2 adsorption equilibrium data.

298 K		323 K		348 K	
f [bar]	q^{abs} [mol kg^{-1}]	f [bar]	q^{abs} [mol kg^{-1}]	f [bar]	q^{abs} [mol kg^{-1}]
0.200	0.066	0.200	0.035	0.200	0.026
0.500	0.138	0.500	0.081	0.510	0.0.66
1.010	0.245	1.010	0.149	1.000	0.106
1.500	0.341	1.510	0.209	1.500	0.151
2.029	0.441	2.000	0.268	2.021	0.197
2.998	0.610	3.030	0.385	3.021	0.295
4.995	0.863	5.010	0.581	5.003	0.443
7.041	1.092	6.999	0.741	7.036	0.577
11.047	1.432	11.019	1.030	11.034	0.802
15.019	1.690	14.999	1.260	15.036	0.984
19.940	1.910	20.010	1.470	20.060	1.170

Table 5. Parameters of CO_2 and N_2 pure component data regressed with Toth equation.

Parameter	Unit	298.15 K		323.15 K		348.15 K	
		Value	Uncertainty [a]	Value	Uncertainty [a]	Value	Uncertainty [a]
CO_2							
Saturation capacity, q_s	mol kg^{-1}	6.06	± 0.159	—	± 0.2790	—	± 0.1650
Henry's law constant, K_H	mol kg^{-1} bar^{-1}	10.77	± 0.128	4.09	± 0.0750	1.92	± 0.0420
Heterogeneity constant, t	—	0.62	± 0.018	0.63	± 0.0310	0.63	± 0.0400
Pre-exponential factor, b_0	(10^{-5}) bar^{-1}	1.06	± 0.078	—	± 0.1160	—	± 0.1430
Monolayer heat of adsorption, E	(−) kJ mol^{-1}	29.78	± 0.182	—	± 0.2950	—	± 0.3950
N_2							
Saturation capacity, q_s	mol kg^{-1}	6.06	± 0.136	—	± 0.1370	—	± 0.2100
Henry's law constant, K_H	mol kg^{-1} bar^{-1}	0.34	± 0.019	0.18	± 0.0001	0.13	± 0.0002
Heterogeneity constant, t	—	0.58	± 0.016	0.62	± 0.0150	0.59	± 0.0200
Pre-exponential factor, b_0	(10^{-5}) bar^{-1}	6.44	± 0.317	—	± 0.0200	—	± 0.0740
Monolayer heat of adsorption, E	(−) kJ mol^{-1}	16.69	± 0.121	—	± 0.0900	—	± 0.0750

A correct fitting at low-pressure region (Henry region) is essential to describe multicomponent data as the integration of reduced grand potential is sensitive to low surface coverage.[29] For this

reason, more data for the strongly adsorbed component were measured at low pressure and at the lowest temperature (see Figure 1a). The isotherms are described well for all temperatures for all systems. At all pressures, carbon dioxide was the most strongly adsorbed gas. Both carbon dioxide and nitrogen isotherms are type I isotherms indicating adsorption of gases in micropores.

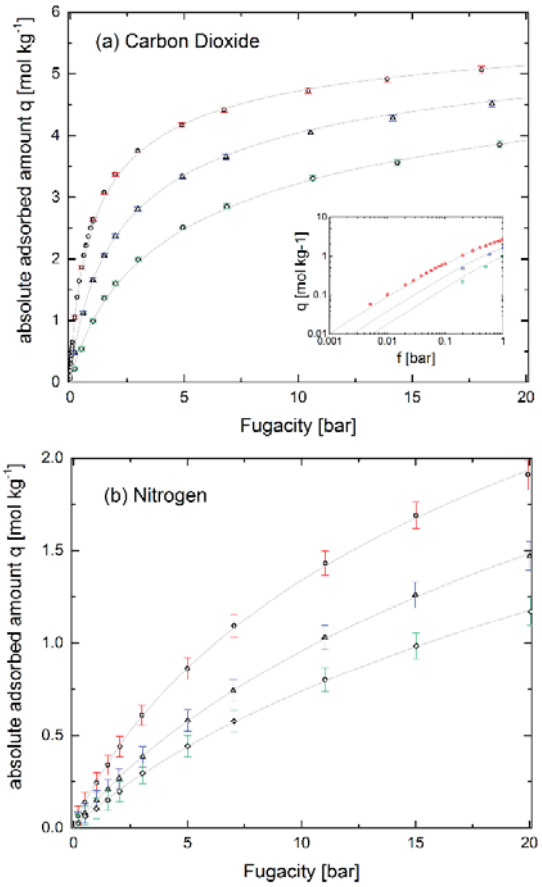

Figure 1. Single component adsorption equilibrium isotherms of: (a) carbon dioxide and (b) nitrogen on AQSOA-FAM-Z02 at: 298.15 K (○), 323.15 K (Δ) and 348.15 K (◊). The solid lines represent the best fit with Toth equation.

Similar CO_2 and N_2 adsorption isotherms on AQSOA-FAM-Z02 were recently reported from Couck et al. [38] for AQSOA-FAM-Z02 powder where 5.6 mol kg^{-1} of pure CO_2 are adsorbed at 303 K and 20 bar. This is slightly higher than the CO_2 uptake on AQSOA-Z02 pellets at the same

conditions that is 5 mol kg^{-1}. N_2 uptakes are instead essentially identical in AQSOA-Z02 powder and pellet.

BINARY MIXTURE ADSORPTION EQUILIBRIA. In order to characterize the co-adsorption behavior of CO_2/N_2, binary adsorption equilibrium gravimetric experiments of CO_2/N_2 were carried out. Experiments for the co-adsorption of CO_2/N_2 mixtures on AQSOA-FAM-Z02 were performed at temperatures from 295 K to 348 K and pressure ranges from the lowest available pressure allowed from the experimental apparatus 1.5–2 bar up to 20 bar. Balance reading in [g], pressure in [bar], temperature in [K], and density in [g cm^{-3}] are listed in Table 6 along with all measured and treated binary data. Predicted results were obtained from the IAST model using the parameters obtained from the single component measurements. Figures 2a, 2b and 2c illustrate the measured and predicted binary adsorption isotherms at temperatures of (295 to 348) K.

As expected from the single component results, CO_2 was the strongly adsorbed component. Therefore, the measured CO_2/N_2 equilibrium compositions were shifted towards higher values as the feed was enriched in CO_2. In addition, the capacities for binary CO_2 adsorption were lower than for pure CO_2. For the sake of simplicity, the CO_2 concentration in the feed stream was plotted against the predicted CO_2 concentration in the adsorbed phase (as obtained from the IAST model) at 323 K and 348 K and is illustrated in Figure 3. According to Figure 3, the concentration of CO_2 in the adsorbed phase is high over an extended range of CO_2 partial pressures. For instance, a 5% CO_2 feed stream gives a >60% concentrated CO_2 in the adsorbed phase at temperatures below 323 K.

Table 6. Experimental adsorption equilibrium data of CO_2/N_2 binary mixture on AQSOA-FAM-Z02.

0.15/0.85 CO_2/N_2 mole fraction				0.5/0.5 CO_2/N_2 mole fraction				0.8/0.2 CO_2/N_2 mole fraction			
T [K]	f [bar]	ρ_{exp} [g cm^{-3}]	q^{abs} [g g^{-1}]	T [K]	f [bar]	ρ_{exp} [g cm^{-3}]	q^{abs} [g g^{-1}]	T [K]	f [bar]	ρ_{exp} [g cm^{-3}]	q^{abs} [g g^{-1}]
295	1.97	0.0024	0.071	295	1.47	0.0021	0.1	297	4.87	0.0081	0.173
295	2.97	0.0037	0.086	295	1.96	0.0028	0.114	297	6.78	0.0116	0.187
295	4.94	0.0061	0.106	295	2.94	0.0043	0.134	297	8.65	0.0150	0.196
295	6.92	0.0086	0.119	295	4.91	0.0072	0.157	297	10.51	0.0186	0.202
295	10.87	0.0135	0.136	295	6.85	0.0101	0.171	297	14.10	0.0258	0.211
295	14.78	0.0184	0.148	295	10.71	0.0161	0.187	297	18.41	0.0351	0.219
295	19.61	0.0246	0.158	295	14.46	0.0222	0.197				
				295	19.05	0.0299	0.206				
323	1.97	0.0022	0.036	323	1.47	0.0019	0.053	323	2.03	0.0029	0.079
323	2.97	0.0033	0.045	323	1.96	0.0025	0.064	323	2.94	0.0043	0.101
323	4.95	0.0055	0.060	323	2.96	0.0039	0.081	323	4.90	0.0073	0.127
323	6.93	0.0078	0.072	323	4.92	0.0065	0.104	323	6.82	0.0104	0.144
323	10.92	0.0122	0.089	323	6.88	0.0092	0.12	323	8.72	0.0136	0.156
323	14.85	0.0167	0.101	323	10.78	0.0146	0.139	323	10.63	0.0168	0.165
323	19.73	0.0223	0.113	323	14.60	0.0201	0.151	323	14.31	0.0233	0.177
				323	19.29	0.0271	0.161	323	18.81	0.0316	0.191
348	1.97	0.0021	0.023	348	1.47	0.0017	0.027	348	2.03	0.0027	0.051
348	2.97	0.0031	0.03	348	1.97	0.0023	0.034	348	2.95	0.004	0.067
348	4.96	0.0052	0.04	348	2.96	0.0035	0.048	348	4.91	0.0068	0.091
348	6.95	0.0073	0.049	348	4.94	0.006	0.068	348	6.84	0.0097	0.108
348	10.95	0.0114	0.062	348	6.9	0.0085	0.083	348	10.71	0.0155	0.131
348	14.93	0.0156		348	10.83	0.0136	0.105	348	14.45	0.0213	0.144
348	19.81	0.0208	0.083	348	14.69	0.0185	0.119	348	19.05	0.0289	0.163
				348	19.45	0.0248	0.131				

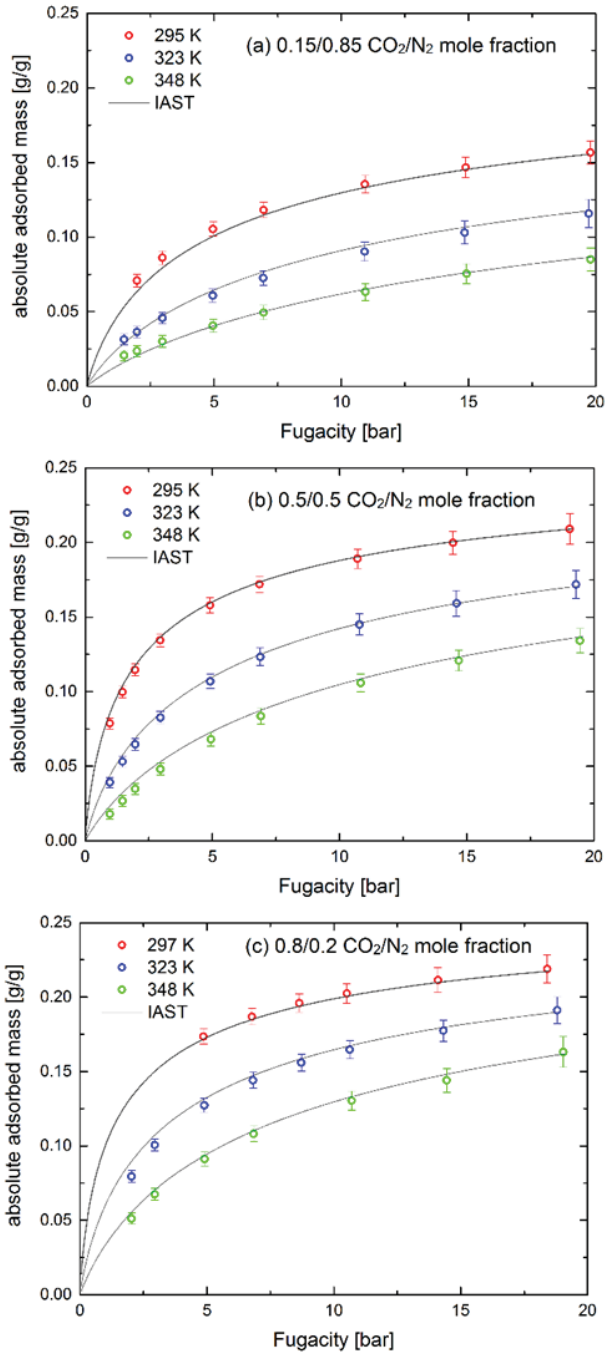

Figure 2. Predicted (lines) and experimental (symbols) binary adsorption equilibria of CO_2/N_2 on AQSOA-FAM-Z02 at (295 to 348) K. Errors were calculated according to Table 2.

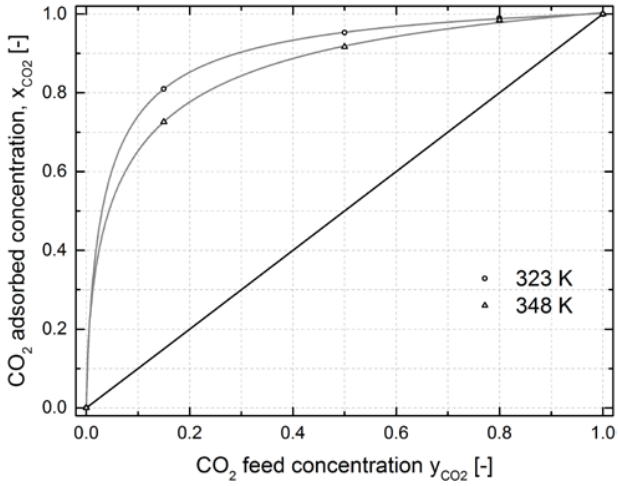

Figure 3. The CO_2 concentration in the gas phase (y_{CO2}) against the predicted CO_2 concentration in the adsorbed phase (x_{CO2}) on AQSOA-FAM-Z02 at 323 K and 348 K.

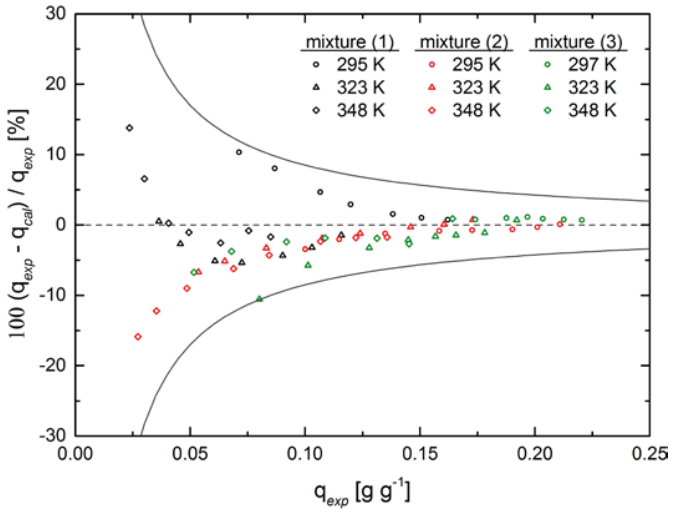

Figure 4. Percent difference between the experimental absolute adsorbed amount and estimated values from IAST: —, estimated uncertainties in the current measurements; ●, mixture (1): 0.15/0.85 CO_2/N_2 mole fraction; ●, mixture (2): 0.50/0.50 CO_2/N_2 mole fraction; and ●, mixture (3): 0.80/0.20 CO_2/N_2 mole fraction.

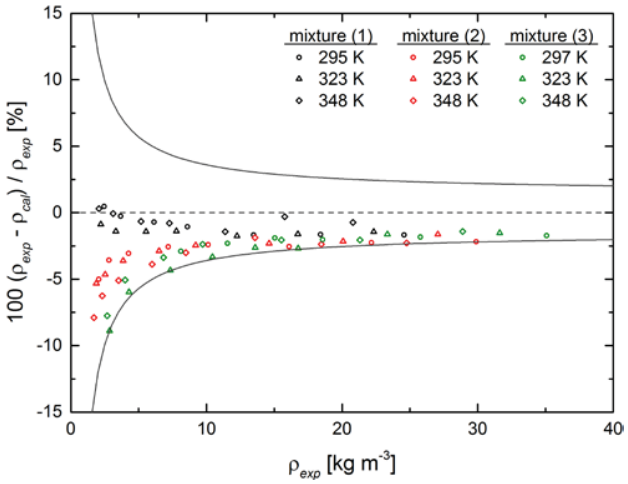

Figure 5. Percent difference between the experimental density and estimated values from REFPROP: —, estimated uncertainties in the current measurements; ●, mixture (1): 0.15/0.85 CO_2/N_2 mole fraction; ●, mixture (2): 0.50/0.50 CO_2/N_2 mole fraction; and ●, mixture (3): 0.80/0.20 CO_2/N_2 mole fraction.

The relative errors ($RE\%$) in the measured absolute adsorbed amount of the CO_2/N_2 mixture on AQSOA-FAM-Z02, defined in eq. (23), are shown in Figure 4

$$RE\% = \left(\frac{q_{exp}-q_{theor}}{q_{exp}}\right) 100 \quad (23)$$

The average relative error ($ARE\%$) in the measured absolute adsorbed amount is

$$ARE\% = \frac{100}{N_{data}} \sum_{i=1}^{N_{data}} \frac{q_{exp}-q_{theor}}{q_{exp}} \quad (24)$$

where the subscripts *"exp"* and *"theor"* denote the experimental and the estimated values. The density of the mixture at each measured pressure step and temperature was also obtained theoretically by means of REFPROP [39] to provide a comparison with the experimental data. The $RE\%$ in density measurements followed eq. (23) and the results are illustrated in Figure 5. Figure 5 shows also the estimated uncertainty in the density measurements, which was found to be ±1.5%

+ 0.21 kg m^{-3}. The maximum $RE\%$ in density was obtained at lower pressures. The deviation in density measurements is mainly due to the uncertainty in pressure, temperature and molar composition analysis and mass and volume measurements of the sinker and the adsorbent. Minor errors, like the force transmission error caused by the magnetic behavior of the cell, the suspension coupling, and the measured fluid, as it had been highlighted Cristancho et al.[40] and Atilhan et al.[41], were not taken into consideration in this study.

Since the fit quality of the pure component isotherms is reasonable, as a <2% $RE\%$ at each measured point was obtained, the discrepancy between the measured and predicted absolute adsorbed amounts (Figure 4) can be explained by the deviation in density measurements (Figure 5). The absolute part of the estimated uncertainty in the density measurements (0.21 kg m^{-3}) explains the higher percent differences at lower density levels.

Table 7. Estimated binary mixture of CO_2 and N_2 adsorption equilibrium data using IAST.

Mixture	T [K]	CO_2 [mmol g^{-1}]	N_2 [mmol g^{-1}]	x_{CO2}[a]	q_{tot} [g g^{-1}][b]	Selectivity
15 mol% CO_2 – 85 mol% N_2	295	0.922	0.137	0.870	0.044	38
	323	0.430	0.101	0.809	0.022	24
	348	0.218	0.083	0.725	0.012	15
50 mol% CO_2 – 50 mol% N_2	295	1.929	0.049	0.975	0.086	39
	323	1.103	0.044	0.962	0.050	25
	348	0.578	0.041	0.934	0.026	14
80 mol% CO_2 – 20 mol% N_2	295	2.217	0.016	0.993	0.098	138
	323	1.462	0.015	0.990	0.065	97
	348	0.864	0.014	0.984	0.038	61

[a] Denotes the molar fraction of CO_2 in the adsorbed phase.
[b] Denotes the total absolute adsorbed amount of the mixture.

The ARE% in the measured amount adsorbed was <4% for each tested CO_2/N_2 mixture at each reported temperature. The estimated uncertainty in the absolute adsorbent amount was found to be

±0.0085 g g^{-1} as illustrated in Figure 4. Therefore, the adsorption data of mixtures can be reasonable described over the entire composition range using the IAST model.

Adsorption selectivity is one of the most important parameters for separation applications. Equilibrium selectivity of CO_2 over N_2 was defined from

$$S_{CO_2/N_2} = \frac{x_{CO_2}/x_{N_2}}{y_{CO_2}/y_{N_2}} \quad (25)$$

Selectivity values are listed in Table 7. Selectivity was increased with the increase of the CO_2 concentration in the feed stream and the reduction in temperature. Accordingly, the highest estimated selectivity was achieved at the 80 mol% CO_2 and 20 mol% N_2 mixture and the lowest reported temperature.

5. CONCLUSIONS

Pure component adsorption and co-adsorption equilibria measurements have been carried out for CO_2, N_2 and their mixtures on AQSOA-FAM-Z02 using a gravimetric apparatus. Single gas isotherms were obtained at pressures between 0.2 bar and 20 bar at (298, 323 and 348) K and were regressed with the Toth isotherm model. CO_2 was found to be the most strongly adsorbed compound with a reported adsorption capacity of 6.1 mmol g^{-1}. Binary adsorption equilibria measurements were performed at pressures from 1.5 bar to 20 bar for different gas compositions at different temperatures. The IAST model in conjunction with the Toth equation was used to predict the adsorbed amount of each gas in the CO_2/N_2 mixture and to characterize the co-adsorption behavior of the mixture. Results showed preferential adsorption of carbon dioxide over nitrogen even at lower concentrations of CO_2. The adsorption loadings for binary CO_2 were lower

than for pure CO_2, which indicates that CO_2 and N_2 adsorbed competitively for the concentration range investigated.

The predictions of binary equilibria with IAST model showed a relatively good agreement with the experimental data giving a <4% $ARE\%$ in the measured absolute adsorbed amounts. The discrepancy between experimental and predicted adsorption equilibrium data at low pressure regions had been explained by the analysis of measurements uncertainties.

AUTHOR INFORMATION

Corresponding Author

* E-mail: g.santori@ed.ac.uk. Tel: +44 (0)131 6519043.

Funding Sources

The research leading to these results was financially supported by EU IRSES (Grant No. 295156), Offshore Gas Separation project (OFFGAS) and EU project Atmospheric Carbon Capture (ACCA, Grant agreement No. 630863).

ACKNOWLEDGMENT

The research leading to these results was financially supported by EU IRSES (Grant No. 295156) Offshore Gas Separation project (OFFGAS) and EU project on Atmospheric Carbon Capture (ACCA, Grant agreement No. 630863).

ABBREVIATIONS

ARE%, average relative error; IAST, ideal adsorbed solution theory; *RE*%, relative error; SSE, sum of squares due to error.

REFERENCES

1. Boot-Handford, M.; Abanades, C.; Anthony, E.; Blunt, M. J.; Brandani, S.; Mac Dowell, N.; Fernández, J. R.; Ferrari, M.-C.; Gross, R.; Hallett, J. P.; Haszeldine, S.; Heptonstall, P.; Lyngfelt, A.; Makuch, Z.; Mangano, E.; Porter, R. T. J.; Pourkashanian, M.; Rochelle, G. T.; Shah, N.; Yao, J.; Fennell, P. Carbon Capture and Storage Update. *Energy Environ. Sci.* **2014**, *7*, 130−189.

2. Samanta, A.; Zhao, A.; Shimizu, G. K. H.; Sarkar, P.; Gupta, R. Post-Combustion CO2 Capture Using Solid Sorbents: A Review. *Ind. Eng. Chem. Res.* **2012**, *51*, 1438−1463.

3. Choi, S.; Drese, J. H.; Jones, C. W. Adsorbent Materials for Carbon Dioxide Capture from Large Anthropogenic Point Sources. *ChemSusChem* **2009**, *2*, 796−854.

4. Ruthven, D. M. Principles of Adsorption and Adsorption Processes; John Wiley & Sons: New York, 1984.

5. Pulin, A. L.; Fomkin, A. A.; Sinitsyn, V. A.; Pribylov, A. A. Adsorption and Adsorption-Induced Deformation of NaX Zeolite under High Pressures of Carbon Dioxide. *Russ. Chem. Bull.* **2001**, *50*, 60–62.

6. Rother, J.; Fieback, T. Multicomponent Adsorption Measurements on Activated Carbon, Zeolite Molecular Sieve and Metal–organic Framework. *Adsorption* **2013**, *19*, 1065–1074.

7. Dunne, J. A.; Rao, M.; Sircar, S.; R. J. Gorte, A.; Myers, A. L. Calorimetric Heats of Adsorption and Adsorption Isotherms. 2. O_2, N_2, Ar, CO_2, CH_4, C_2H_6, and SF_6 on NaX, H-ZSM-5, and Na-ZSM-5 Zeolites. *Langmuir*. **1996**, *12*, 5896–5904.

8. Hefti, M.; Marx, D.; Joss, L.; Mazzotti, M. Adsorption Equilibrium of Binary Mixtures of Carbon Dioxide and Nitrogen on Zeolites ZSM-5 and 13X. *Micropor. Mesopor. Mater*. **2015**, *215*, 215–228.

9. Harlick, P. J. E.; Tezel, F. H. An Experimental Adsorbent Screening Study for CO_2 Removal from N_2. *Micropor. Mesopor. Mater*. **2004**, *76*, 71–79.

10. Joos, L.; Swisher, J. A.; Smit, B. Molecular Simulation Study of the Competitive Adsorption of H_2O and CO_2 in Zeolite 13X. *Langmuir* **2013**, *29*, 15936–15942.

11. Lee, K. B.; Sircar, S. Removal and recovery of compressed CO_2 from flue gas by a novel thermal swing chemisorption process. *AIChE J*. **2008**, *54*, 2293–2302.

12. Sing, K. S. W.; Everett, D. H.; Haul, R. A. W.; Moscou, L.; Pierotti, R. A.; Rou- querol, J.; Siemieniewska, T. Reporting ph- ysisorption data for gas/solid systems with special reference to the determination of sur- face area and porosity. *Pure Appl. Chem*. **1985**, *57*, 603–619.

13. Mitsubishi Plastics Inc., Business Development Dep. Industrial Materials Division, Zeolitic Water Vapor Adsorbent AQSOA^{TM}. 2008, pp 1–4; *http://www.mpi.co.jp/infopdf/AQSOA.pdf*.

14. Goldsworthy, M. J. Measurements of Water Vapour Sorption Isotherms for RD Silica Gel, AQSOA-Z01, AQSOA-Z02, AQSOA-Z05 and CECA Zeolite 3A. *Micropor. Mesopor. Mater*. **2014**, *196*, 59–67.

15. Wei Benjamin Teo, H.; Chakraborty, A.; Fan, W. Improved adsorption characteristics data for AQSOA types zeolites and water systems under static and dynamic conditions. *Micropor. Mesopor. Mat.* **2017**, 242, 109–117.

16. Lackner, K. S. Capture of carbon dioxide from ambient air. *Eur. Phys. J. Special Topics* **2009**, *176*, 93–106.

17. ElSherif, D.; Knox, J. C. International Space Station Carbon Dioxide Removal Assembly (ISS CDRA) Concepts and Advancements. International Conference on Environmental Systems. Rome, 2005; pp 1–5.

18. Sapienza, A.; Santamaria, S.; Frazzica, A.; Freni, A. Influence of the Management Strategy and Operating Conditions on the Performance of an Adsorption Chiller. *Energy* **2011**, *36*, 5532–5538.

19. Santori, G.; Frazzica, A.; Freni, A.; Galieni, M.; Bonaccorsi, L.; Polonara, F.; Restuccia, G. Optimization and testing on an adsorption dishwasher. *Energy* **2013**, *50*, 170–176.

20. Mitsubishi Plastics Inc., Industrial Materials Zeolite AQSOA™. 1962; http://www.mpi.co.jp/english. (accessed Aug 29, 2017)

21. Kayal, S.; Baichuan, S.; Saha, B. B. Adsorption Characteristics of AQSOA Zeolites and Water for Adsorption Chillers. *Int. J. Heat Mass Transf.* **2016**, *92*, 1120–1127.

22. Brandani, S.; Mangano, E.; Sarkisov, L. Net, excess and absolute adsorption and adsorption of helium. *Adsorption* **2016**, *22*, 261–276.

23. Weireld, G. D.; Frère, M.; Jadot, R. Automated determination of high-temperature and high-pressure gas adsorption isotherms using a magnetic suspension balance. *Meas. Sci. Technol.* **1999**, *10*, 117–126.

24. Dreisbach, F.; Lösch, H. W.; Harting, P. Highest Pressure Adsorption Equilibria Data: Measurement with Magnetic Suspension Balance and Analysis with a New Adsorbent/Adsorbate-Volume. *Adsorption* **2002**, *8* (2), 95–109.

25. Bezerra, D. P.; Oliveira, R. S.; Vieira, R. S.; Cavalcante, C. L.; Azevedo, D. C. S. Adsorption of CO_2 on Nitrogen-Enriched Activated Carbon and Zeolite 13X. *Adsorption* **2011**, *17*, 235–246.

26. Vilarrasa-García, E.; Cecilia, J. A.; Bastos-Neto, M.; Cavalcante, C. L.; Azevedo, D. C. S.; Rodriguez-Castellón, E. CO_2/CH_4 Adsorption Separation Process Using Pore Expanded Mesoporous Silicas Functionalizated by APTES Grafting. *Adsorption* **2015**, *21*, 565–575.

27. May, E. F.; Miller, R. C.; Shan, Z. Densities and Dew Points of Vapor Mixtures of Methane + Propane and Methane + Propane + Hexane Using a Dual-Sinker Densimeter. *J. Chem. Eng. Data* **2001**, *46*, 1160–1166.

28. McLinden, M. O.; Lösch-Will, C. Apparatus for wide-ranging, high-accuracy fluid (p,ρ,T) measurements based on a compact two-sinker densimeter. *J. Chem. Thermodynamics* **2007**, *39*, 507–530.

29. Myers, A. L.; Monson, P. A. Physical adsorption of gases: the case for absolute adsorption as the basis for thermodynamic analysis. *Adsorption* **2014**, *20*, 591–622.

30. Vilarrasa-García, E.; Cecilia, J. A.; Rodríguez Aguado, E.; Jiménez-Jiménez, J.; Cavalcante, C. L.; Azevedo, D. C. S.; Rodríguez-Castellón, E. Amino-modified pillared adsorbent from water-treatment solid wastes applied to CO2/N2 separation. Adsorption 2017, 23, 405–421.

31. Pini, R. Interpretation of Net and Excess Adsorption Isotherms in Microporous Adsorbents. *Micropor. Mesopor. Mater.* **2014**, *187*, 40–52.

32. Lowell, S., Shields, J.E., Thomas, M.A., Thommes, M. Characterization of Porous Solids and Powders: Surface Area, Pore Size and Density. 2004. Kluwer Academic Publishers. Edition 1.

33. Saleh, B.; Wendland, M. Measurement of Vapor Pressures and Saturated Liquid Densities of Pure Fluids with a New Apparatus. *J. Chem. Eng. Data* **2005**, *50*, 429–437.

34. Do, D. D. *Adsorption Analysis: Equilibria and Kinetics*, second ed.; Imperial College Press, 1998; pp 1–892.

35. Wang, Y.; LeVan, M. D. Adsorption Equilibrium of Carbon Dioxide and Water Vapor on Zeolites 5A and 13X and Silica Gel: Pure Components. *J. Chem. Eng. Data* **2009**, *54*, 2839–2844.

36. Santori, G.; Luberti, M.; Brandani, S. Common tangent plane in mixed-gas adsorption. *Fluid Phase Equilibr.* **2015**, *392*, 49–55.

37. Santori, G.; Luberti, M.; Ahn, H. Ideal adsorbed solution theory solved with direct search minimisation. *Comput. Chem. Eng.* **2014**, *71*, 235–240.

38. Couck, S.; Cousin-Saint-Remi, J.; Van der Perre, S.; Baron, G. V.; Minas, C.; Ruch, P.; Denayer, J. F. 3D-printed SAPO-34 monoliths for gas separation. *Micropor. Mesopor. Mat.* **2018**, *255*, 185–191.

39. Lemmon, E. W.; Huber, M. L.; McLinden, M. O. NIST Standard Reference Database 23: Reference Fluid Thermodynamic and Transport Properties-REFPROP, Version 9.1, National Institute of Standards and Technology. 2013; https://www.nist.gov/srd/refprop. (accessed Jan 08, 2018)

40. Cristancho, D. E.; Mantilla, I. D.; Ejaz, S.; Hall, K. R.; Iglesias-Silva, G. A.; Atilhan, M. Force transmission error analysis for a high- pressure single-sinker magnetic suspension densimeter. *Int. J. Thermophys*. **2010**, *31*, 698–709.

41. Atilhan, M.; Ejaz, S.; Zhou, J.; Cristancho, D.; Mantilla, I.; Holste, J.; Hall, K. R. Characterization of Deepwater Natural Gas Samples. Part 1: 78% Methane Mixture with Heavy Components. *J. Chem. Eng. Data* **2010**, *55*, 4907–4911.

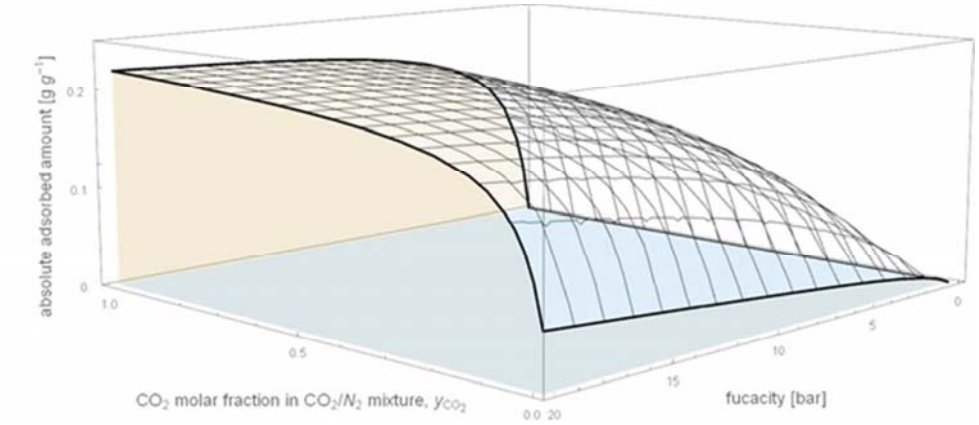

For Table of Contents Only

165x71mm (96 x 96 DPI)